High-Temperature Materials

SCIEPublish

Review

A Review of Heat-Resistant Al Alloys: Strengthening Strategies and Processing Technologies

Yi-Nan Piao [1], Hai-Long Jia [1,2,*], Tian-Yue Li [1], Jia-Wang Song [1], He Wei [3] and Min Zha [1,2,*]

[1] Key Laboratory of Automobile Materials of Ministry of Education & School of Materials Science and Engineering, Nanling Campus, Jilin University, No. 5988 Renmin Street, Changchun 130025, China; piaoyn25@mails.jlu.edu.cn (Y.-N.P.); tyli24@mails.jlu.edu.cn (T.-Y.L.); songjw@jlu.edu.cn (J.-W.S.)

[2] International Center of Future Science, Jilin University, Changchun 130012, China

[3] Faculty of Materials Science and Engineering, Kunming University of Science and Technology, Kunming 650093, China; Weihe@kust.edu.cn (H.W.)

* Corresponding author. E-mail: jiahailong@jlu.edu.cn (H.-L.J.); minzha@jlu.edu.cn (M.Z.)

Received: 20 July 2026; Revised: 10 August 2026; Accepted: 28 August 2026; Available online: 15 September 2026

ABSTRACT: The rapid advancement of aerospace and transportation technologies toward weight reduction and harsh thermal environments has imposed a stringent demand for Al alloys that can sustain excellent performance at 200–400 °C. Heat-resistant Al alloys have thus garnered strategic significance as a premier class of lightweight structural materials for elevated-temperature applications. This review critically assesses the current state of heat-resistant Al alloys from the perspectives of strengthening strategies and processing technologies. Three representative strengthening strategies have been summarized, including multi-element microalloying, incorporation of nanoparticles, and formation of nano-eutectic skeleton. Meanwhile, a systematic comparative analysis has been conducted on microstructural regulations and mechanical properties of alloys manufactured by permanent mold casting (PMC), powder metallurgy (PM), and laser powder bed fusion (LPBF), with particular emphasis on the processing-structure-property correlations unique to each route. On this basis, the principal technical bottlenecks currently constraining the further advancement of high-performance heat-resistant Al alloys have been identified and critically discussed, thereby outlining prospective research directions to overcome these limitations.

Keywords: Heat-resistant Al alloy; Strengthening strategy; Processing technology; Microstructural regulation; Mechanical property

1. Introduction

With the rapid advancement of aero-engines and other high-end equipment, there is an increasingly urgent demand for metallic materials with excellent high-temperature resistance [1]. These practical applications require materials that combine high strength, low density, and outstanding high-temperature performance. Although Ni-based superalloys still dominate for service above 600 °C (such as aero-engine combustion chambers), the demand for dedicated structural materials targeting the 200–400 °C temperature window keeps rising. Table 1 summarizes the extreme-service conditions of representative components

© 2026 The authors. This is an open access article under the Creative Commons Attribution 4.0 International License (https://creativecommons.org/licenses/by/4.0/).

from different industrial fields. Lightweight heat-resistant Al alloys are core structural materials for high-end aerospace components operating at 200–400 °C, offering significant weight reduction advantages over Ti alloys and steel components [2–4]. Conventional 2xxx, 6xxx, and 7xxx series cast Al alloys rely primarily on nano-scale precipitates such as θ′, β′, Ω, and Q′ for strengthening [5–7]. However, these precipitates undergo severe dissolution and Ostwald ripening above 200 °C, leading to a dramatic degradation in tensile strength and creep resistance. The insufficient thermal stability of these precipitates restricts the maximum service temperature of current commercial Al alloys to only ~150 °C, far below the high-temperature requirements of supersonic aircraft and aero-engine components.

Table 1. Alloys are commonly employed for components under different service conditions.

Field	Component	Operating Temp. (°C)	Loading Type	Environmental Resistance	References
Aircraft engines (Ni-based alloys)	Combustion chamber	600–1000	High-temperature static load/Cyclic thermal fatigue	High-temperature oxidation/Corrosion	[8–10]
Aircraft engines (Ti alloys)	Fan disk	400–600	Cyclic thermal fatigue	High-temperature oxidation/Corrosion	[8]
Internal combustion engines (Al alloys)	Piston	−30–250	Cyclic thermal fatigue	High-temperature oxidation/Corrosion/Abrasive wear	[11,12]
New energy battery (Al alloys)	Battery case	−30–80	Vibration load/Mechanical impact load/Cyclic thermal fatigue	Corrosion/Sealing failure/Thermal runaway impact	[13]

In recent years, with deepening research and the emergence of new technologies, the service temperature of heat-resistant Al alloys has been progressively elevated, and novel alloys capable of operating at 400 °C have been successfully developed, laying a solid foundation for the heat-resistant and high-strength Al alloys urgently needed in the aerospace field. Enhancing the high-temperature mechanical properties of Al alloys depends on two principal routes: introducing thermally stable strengthening phases and innovating processing technologies to achieve microstructural regulations. Currently, microalloying remains the mainstream strategy in research on heat-resistant Al alloys, *i.e.*, introducing minor alloying elements either to form new heat-resistant strengthening phases that pin dislocations and grain boundaries or to suppress precipitate coarsening through interfacial segregation, thereby enhancing high-temperature mechanical properties [14,15]. Meanwhile, laser powder bed fusion delivers cooling rates far higher than those of traditional solidification techniques, enabling refined microstructures and near-net-shape manufacturing of large-scale complex aerospace components [16,17], which has become a leading technology for fabricating eutectic heat-resistant Al alloy components [18–20].

This review systematically summarizes three mainstream strengthening strategies for heat-resistant Al alloys, including multi-element microalloying, incorporation of nanoparticles, and formation of nano-eutectic skeleton (Figure 1). It thoroughly compares intrinsic differences among permanent mold casting (PMC), powder metallurgy (PM), and laser powder bed fusion (LPBF) processes in terms of solidification characteristics, microstructural regulations, and mechanical properties. Furthermore, it summarizes current bottlenecks and future directions for development, aiming to provide a systematic theoretical basis for the design of novel heat-resistant Al alloys for use in extreme thermal environments.

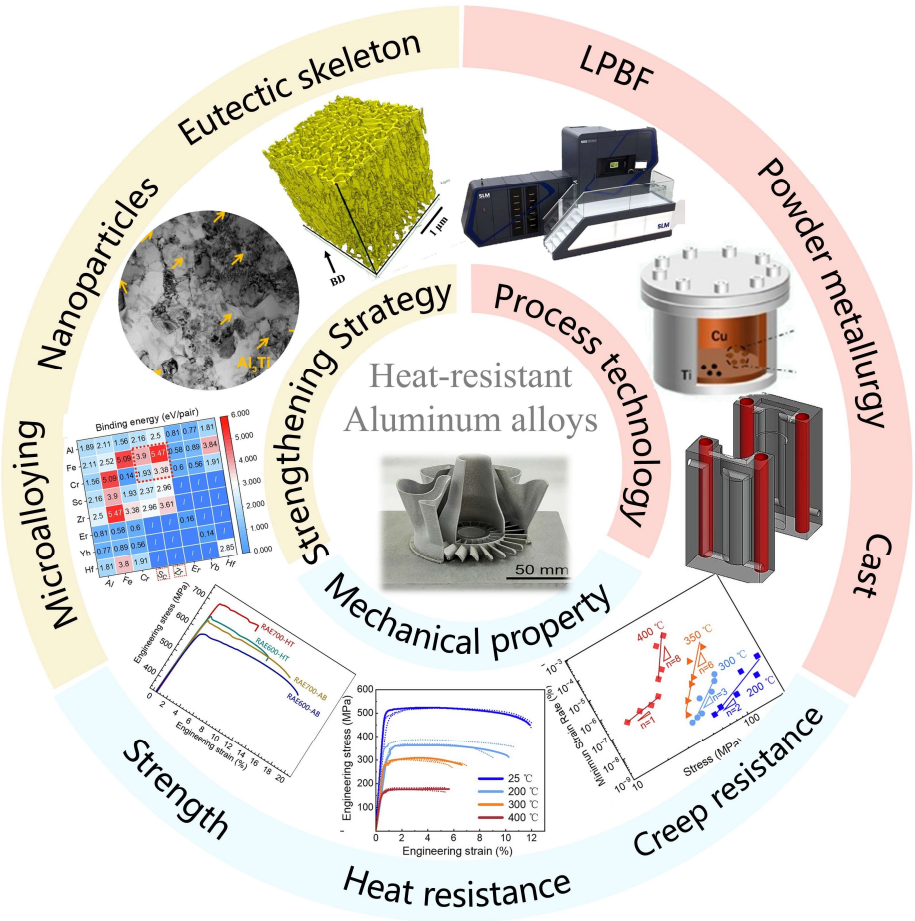

Figure 1. Schematic diagram illustrating the overall research framework of heat-resistant Al alloys, including typical strengthening strategies (Reprinted with permission from Ref. [21–23]. Copyright 2025, and 2026, Springer Nature), (the red dashed lines denote microalloying elements optimized via theoretical calculations), mainstream processing technologies (Reprinted with permission from Ref. [24–26]. Copyright 2022, 2026, and 2025, Elsevier, Taylor & Francis, and MDPI), and mechanical properties (Reprinted with permission from Ref. [18,21]. Copyright 2026, Springer Nature).

2. Strategies for Improving Heat-Resistant Properties of Al Alloys

As shown in Figure 2a–d, conventional strengthening approaches widely adopted for Al alloys consist of solid solution strengthening [27], grain boundary strengthening [28,29], precipitation strengthening [30], and dislocation strengthening [31]. All these methods achieve superior material performance by enhancing the resistance to dislocation motions. The high-temperature strengthening mechanisms of heat-resistant Al alloys exhibit great similarity to the conventional mechanisms described above. This section reviews the most representative design strategies for improving heat-resistant properties of Al alloys developed under various manufacturing routes, including PMC, PM, and LPBF. In this review, the three strengthening strategies are classified according to the formation mechanisms and the morphological features of strengthening phases. Multi-element microalloying produces *in-situ* nano-sized precipitates or interfacial segregation from supersaturated solid solutions during aging, relying on heat treatments. Nanoparticle incorporation achieves extrinsic dispersion strengthening by mechanically embedding externally synthesized, thermally stable ceramic nanoparticles. Nano-eutectic skeleton construction generates interconnected nano-eutectic networks *in-situ* through eutectic solidification under the extreme non-equilibrium conditions of LPBF, forming continuous reinforcing frameworks that are distinctly different from discrete precipitates or isolated extrinsic nanoparticles. Although the three strategies are not mutually exclusive and may be combined in principle, they differ fundamentally in the origin and morphology of the main strengthening phases. Accordingly, they are treated as three independent paradigms in this review.

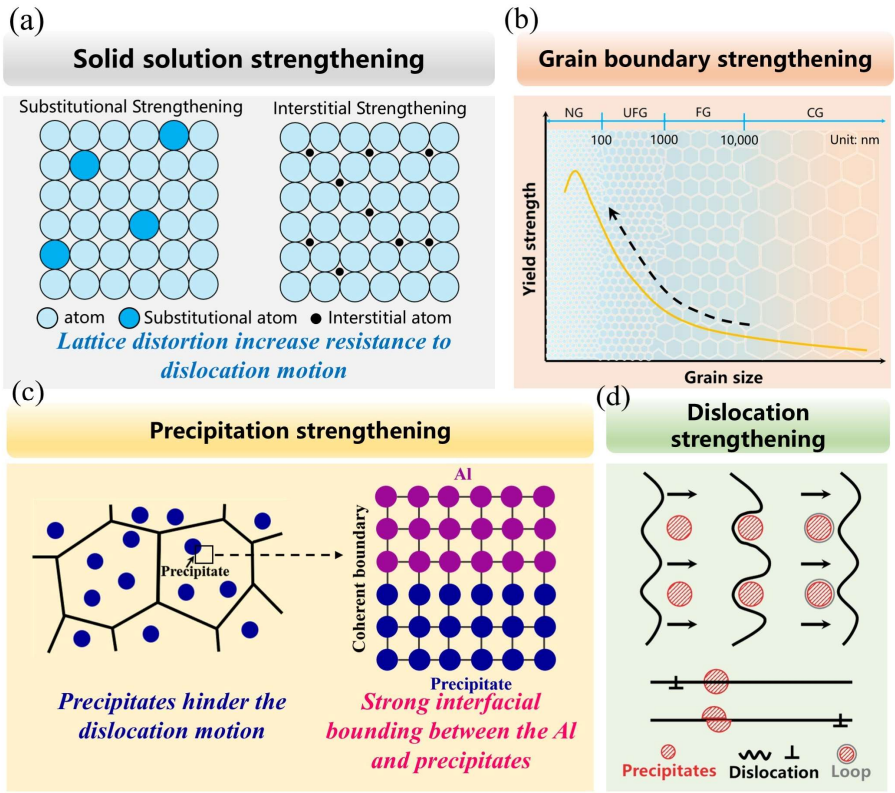

Figure 2. Schematics illustrating four strengthening mechanisms: (**a**) solid solution strengthening; (**b**) grain boundary strengthening; (**c**) precipitation strengthening; (**d**) dislocation strengthening. Arrows in (**b**) show the rising trend, while those in (**d**) indicate the direction of dislocation motion.

2.1. Microalloying

Microalloying introduces trace solutes into heat-resistant Al alloys to precisely tailor the type, morphology, and number density of precipitates, substantially boosting their high-temperature mechanical performance. Three dominant microalloying strategies have been established: (i) constructing multicomponent thermally stable precipitates via synergistic interaction between major and trace solutes [32]; (ii) stabilizing nanoprecipitates by interfacial solute segregation [15,33]; (iii) inhibiting precipitate coarsening via solute-vacancy interaction [21].

2.1.1. Thermally Stable Precipitate Type Design

Conventional nanoprecipitates in age-hardened Al alloys, such as θ′, β′, Q′, Ω, and η′ precipitates (Figure 3a–d), deliver substantial strength at room temperature. However, they undergo severe coarsening and dissolution at temperatures above 200 °C, which limits their use in aerospace components. Commercial high-strength Al alloys currently offer a maximum service temperature of only ~150 °C. The core limitation lies in the difficulty of obtaining coherent nanoprecipitates that simultaneously exhibit outstanding thermal stability and a high volume fraction. Although the addition of trace elements such as Sn [34] and Cd [35] can promote dense, dispersed precipitation through heterogeneous nucleation, such alloying strategies yield only marginal improvements in high-temperature performance and fail to fundamentally overcome the intrinsically poor thermal stability of precipitates.

Surprisingly, Sc substantially improves the thermal resistance of Al alloys. Differing from simple interfacial segregation, Sc participates in *in-situ* phase transformation at elevated temperatures. In Al–Cu–Mg–Ag–Sc alloys [32], a high-volume fraction of Ω nanoprecipitates forms via fast-diffusing Cu solutes. Following two-stage ageing, slow-diffusing Sc atoms penetrate the interior of Ω precipitates through

coherent ledges, occupying interstitial lattice sites and fully transforming Ω into thermally robust V-phase nanoparticles. The phase transformation retains a high precipitate number density and drastically improves intrinsic thermal stability. It retains a high number density of precipitates while substantially improving their intrinsic thermal stability.

While conventional precipitates (θ′, β′, Q′) provide substantial room-temperature strength, they suffer from rapid coarsening at temperatures exceeding 200 °C. By contrast, the Ω phase maintains coherency up to 200 °C. Additionally, the V phase forms via Sc interstitial ordering, extending the stable service temperature to 400 °C. At 400 °C, its coarsening rate is nearly two orders of magnitude lower than that of the θ′ phase. This significant disparity highlights the essential roles of solute diffusion control and interfacial engineering in surmounting the persistent temperature limitation of precipitation-strengthened Al alloys.

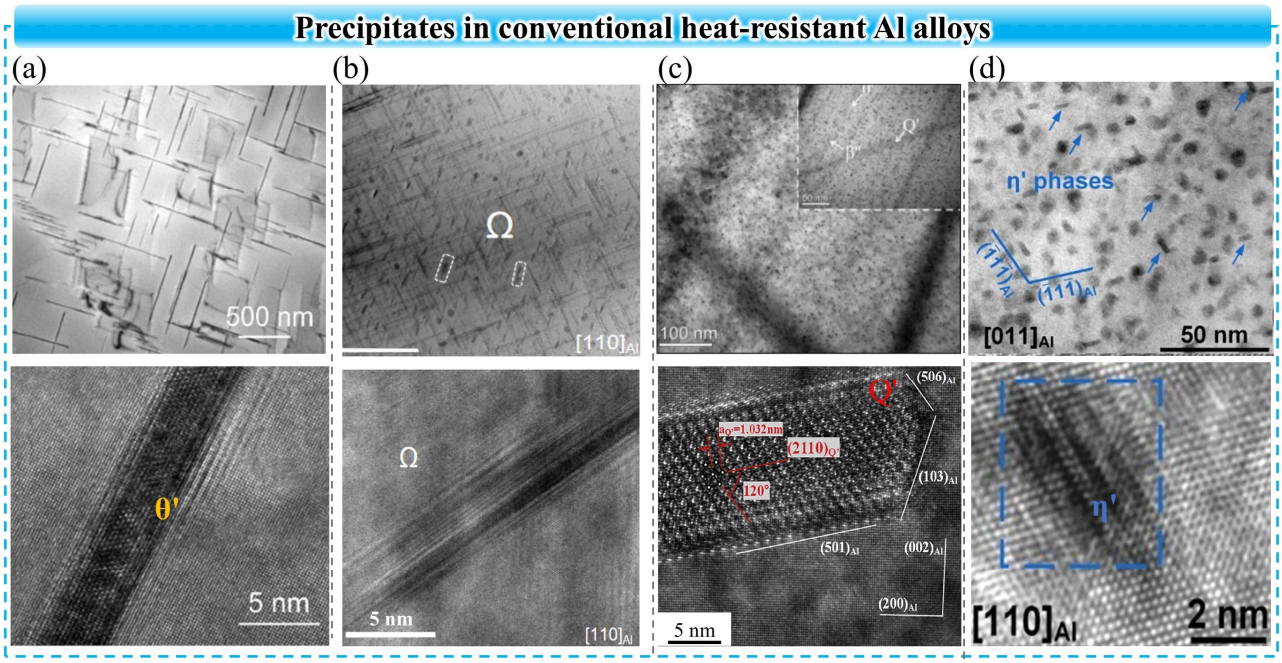

Figure 3. The TEM and HRTEM results of precipitates in conventional Al alloys: (**a**) θ′ precipitates in Al–Cu alloy (Reprinted with permission from Ref. [36]. Copyright 2020, Taylor & Francis); (**b**) Ω precipitates in Al–Cu–Mg alloy (Reprinted with permission from Ref. [37]. Copyright 2026, MDPI); (**c**) Q′ precipitates in Al–Si–Cu–Mg alloy (Reprinted with permission from Ref. [5]. Copyright 2023, Elsevier); (**d**) η′ precipitates in Al–Zn–Mg–Cu–Si alloy (Reprinted with permission from Ref. [38]. Copyright 2025, Taylor & Francis).

2.1.2. Interfacial Solute Segregation for Precipitate Stabilization

Solute segregation at precipitate/matrix interfaces can effectively improve the strength and thermal stability [39]. In Sc-modified Al–Cu alloys, as a representative alloy, a high-volume fraction of plate-like θ′-Al_2Cu nanoprecipitates forms after aging. Three-stage heat treatment introduces Sc-segregated layers at precipitate interfaces, forming sandwich thermal barrier structures that significantly suppress precipitate growth (Figure 4a). This structure serves as a thermal barrier and markedly enhances high-temperature mechanical properties [36]. Additionally, Ag has also been found to segregate at precipitate/matrix interfaces in Al–Cu alloys [15,40]. The fully coherent $(001)_{\theta'}//(001)_{Al}$ interface is decorated by an ordered double Ag atomic segregation bilayer, which suppresses the lateral growth of θ′ precipitates (Figure 4b). Nevertheless, single-solute segregation layers cannot fully restrain Ostwald ripening under long-term high-temperature exposure. Composite multi-solute interfacial structures represent a more promising solution. In Al–Cu–Mg–Ag–Si–Sc alloys [33], Sc segregation layers, C/L phases, and χ-AgMg interphase collectively coat θ′ precipitates (Figure 4e). This multi-layer sandwich structure further reduces interfacial

energy via solute synergies. After thermal exposure at 210 °C for 100 h, the average thickness of the θ′ precipitates only slightly rises from 2.8 ± 0.8 nm to 2.9 ± 0.7 nm. It shows negligible coarsening, verifying the excellent stabilizing effect of composite segregation (Figure 4c,d). This design strategy of coating nanoprecipitates with a hybrid network of multi-type interfacial phases and solute segregation layers delivers an effective framework for developing a broad range of heat-resistant Al alloys.

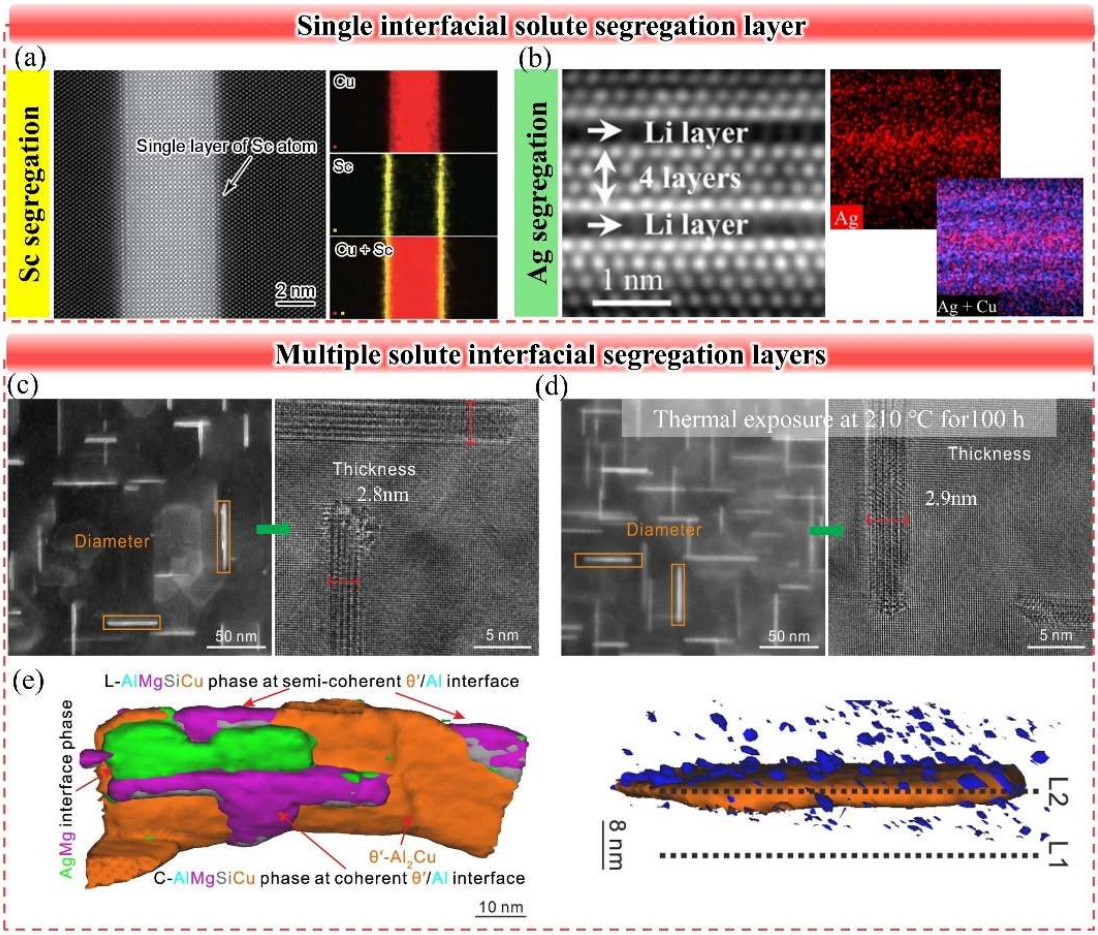

Figure 4. HAADF and EDS results of single interfacial solute segregation layer in Al–Cu alloys: (**a**) Sc solute segregation (Reprinted with permission from Ref. [36]. Copyright 2020, Taylor & Francis); (**b**) Ag solute segregation (Reprinted with permission from Ref. [40]. Copyright 2025, Taylor & Francis). HAADF and APT analyses of multiple solutes interfacial segregation layers in Al–Cu–Mg–Ag–Si–Sc alloys (Reprinted with permission from Ref. [33]. Copyright 2023, Springer Nature); (**c**) the peak-ageing state; (**d**) thermal exposure at 210 °C for 100 h; (**e**) multiple interface phases and segregation layers at θ′/Al interfaces.

2.1.3. Solute-Vacancy Interaction Stabilization Strategy

High-temperature service environments induce vacancy migration and rapid solute diffusion within the Al matrix, which consequently leads to precipitate coarsening and mechanical property degradation of LPBF heat-resistant Al alloys [41,42]. Traditional alloy design merely relies on slow-diffusing substitutional solutes to retard phase coarsening. By contrast, the solute-vacancy interaction stabilization strategy constructs thermodynamically stable solute-vacancy complexes that suppress diffusion at the atomic scale (Figure 5a), providing a new microstructural control concept for LPBF heat-resistant Al alloys [43]. The ultra-fast cooling inherent to LPBF retains a large population of supersaturated vacancies, and the addition of Cr, Fe, Sc, and Zr enables the formation of multi-element solute-vacancy clusters with high binding energy (Figure 5b), which trap free vacancies and block rapid atomic diffusion pathways [21]. Simultaneously, segregation of Cr, Fe, Sc, and Zr at $L1_2$–Al_3(Sc, Zr) and Al_{13}(Fe, Cr) phase interfaces

forms diffusion barriers that inhibit coarsening. Cr traps vacancies to form solute-vacancy clusters, suppressing vacancy-mediated diffusion. Fe/Cr form solute atmospheres that drag dislocations and inhibit climb. Sc/Zr segregate at phase interfaces, reducing interfacial energy and suppressing Ostwald ripening. This mechanism achieves a better balance between high-temperature strength and ductility.

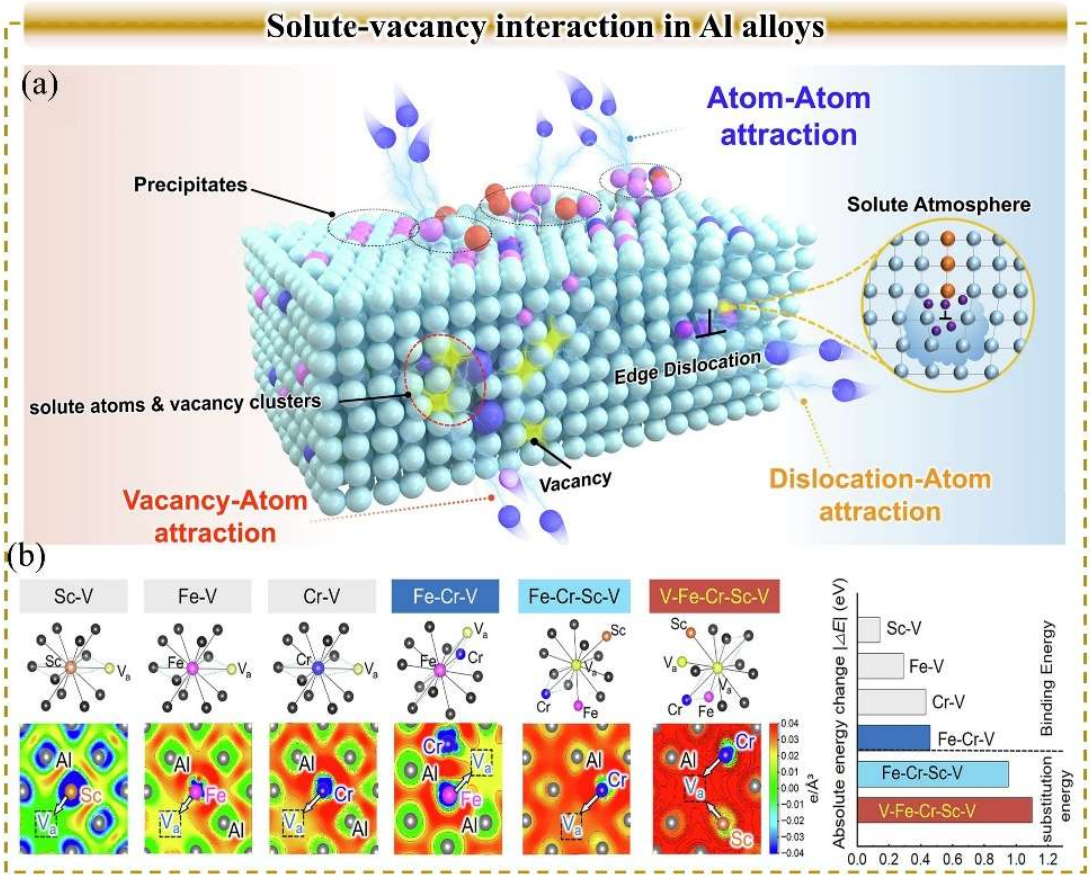

Figure 5. The intrinsic attraction strategy in LPBF-fabricated Al–Fe–Cr–Sc–Zr alloys (Reprinted with permission from Ref. [21]. Copyright 2026, Springer Nature): (**a**) diagram for the intrinsic attraction strategy against thermally driven defect mobilization (to suppress thermally induced defect mobilization, defects (e.g., vacancies, dislocations) are regulated and anchored by exploiting strong intrinsic solute–defect attractions, thereby retaining sufficient immobile defects at elevated temperatures); (**b**) deformation charge density difference maps of monatomic-monovacancy and binding energy.

2.2. Nanoparticle-Incorporation Strengthening Strategy

Nanoparticle-incorporation strengthening relies on thermodynamically stable nanoparticles uniformly dispersed in the Al matrix to maintain microstructural stability at elevated temperatures [44]. The dominant Orowan bypass mechanism involves high-melting dispersoids (e.g., TiC, MgO, and Y_2O_3) that strongly pin dislocations and grain boundaries [45]. This imparts nanoparticle-incorporation strengthening Al alloys with markedly superior thermal stability and creep resistance compared to age-hardened Al alloys. Unlike precipitates formed by artificial aging, ceramic nanoparticles retain constant size, morphology, and high-volume fraction even above 450–500 °C, thereby eliminating dissolution and Ostwald ripening. Conventional mechanical alloying for fabricating high-performance nanoparticle-incorporation strengthening Al alloys often induces severe agglomeration of nanoparticles, generating micro-void defects and drastically deteriorating the ductility of the alloy.

Recent advances in powder metallurgy have overcome these limitations. Interfacial modification and core-shell pre-dispersion strategies (e.g., graphite-coated MgO nanoparticles) reduce inter-particle adhesion by 2–3 orders of magnitude, enabling homogeneous dispersion of individual 5 nm MgO particles

throughout the Al matrix [46]. The fully coherent MgO/Al interfaces block vacancy diffusion pathways along phase boundaries. Consequently, these Al alloys retain a tensile strength exceeding 200 MPa after thermal exposure at 500 °C. Additionally, Hu et al. [22] fabricated hierarchical Al_3Ti/Al matrix composites via controlled *in-situ* reactions between layered Ti_2AlC phase precursor and Al matrix assisted by high-energy ball milling (Figure 6a). This process creates a dual-pathway diffusion architecture, triggering internal decomposition of Ti_2AlC and producing a hierarchical structure with ~6 vol.% Al_3Ti particles (coherent between Al_3Ti/Al) uniformly dispersed in Al matrix. (Figure 6b,c), The resulting composites exhibit outstanding elevated-temperature strength, with ultimate tensile strengths of 632 MPa (at 25 °C) and 246 MPa (at 350 °C).

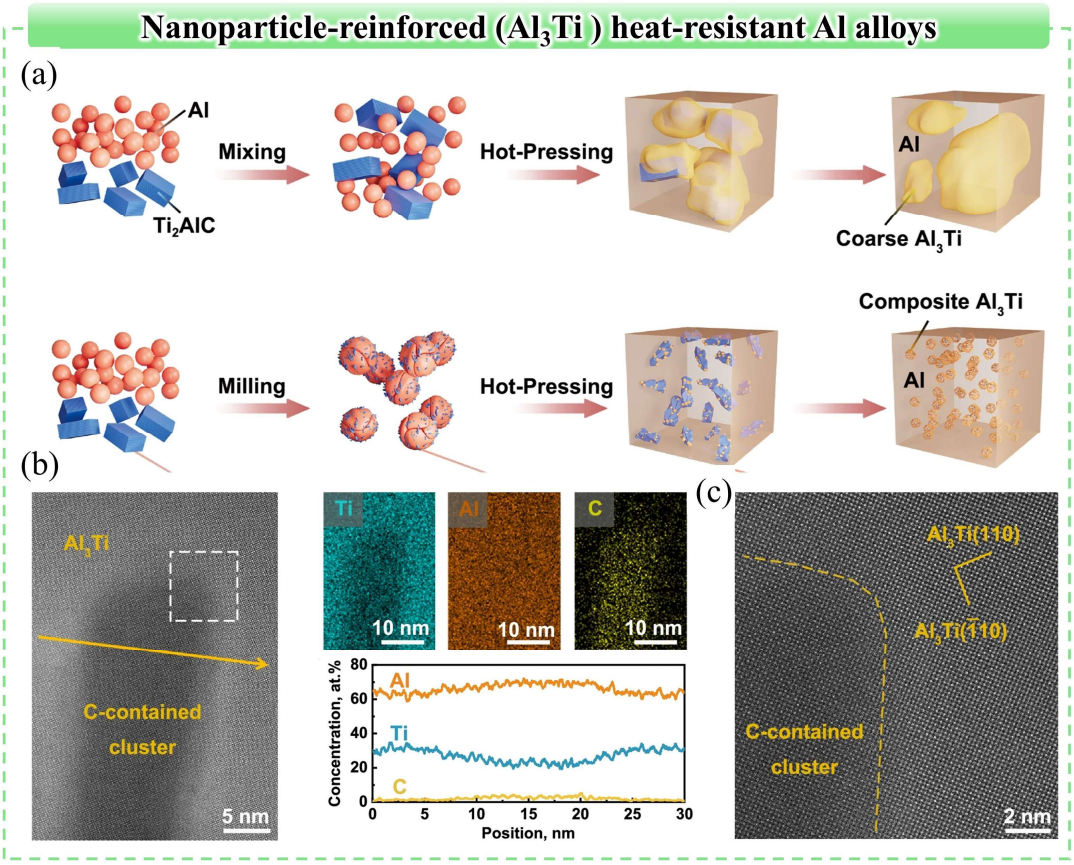

Figure 6. The fabrication and microstructures of nanoparticle-reinforced heat-resistant Al alloys (Reprinted with permission from Ref. [22]. Copyright 2026, Springer Nature): (**a**) schematic showing dispersion process by ordinary powder mixing and mechanical force during ball-milling; (**b**) HRTEM and EDS images of the coherent between Al_3Ti/Al matrix (yellow arrow denotes the line-scan region); (**c**) a magnified view of the white rectangle in (**b**).

2.3. Nano-Eutectic Skeleton Strategy Enabled by LPBF

The development of LPBF technology has substantially broadened the high-temperature performance window of Al alloys. The layer-by-layer solidification inherent to LPBF achieves extremely high cooling rates of 10^6–10^8 K/s, enabling a design strategy for heat-resistant Al alloys based on the formation of nanoscale eutectic skeleton through rapid solidification [17]. Under such extreme non-equilibrium conditions, the coarse equilibrium eutectic phases typically formed in conventional casting are effectively avoided. Instead, a three-dimensionally nano-eutectic network forms within α-Al grains and along grain boundaries. The rigid nano-framework, composed of rare-earth or transition-metal intermetallics (e.g., Al–La, Al–Er, Al–Ni), exerts a dual strengthening effect at elevated temperatures (Figure 7). On the one hand, the high-density eutectic network generates a strong pinning force that inhibits grain boundary migration

and dislocation climb. On the other hand, the eutectic phases that penetrate the matrix exhibit a portion of the applied load through load transfer, thereby significantly enhancing the high-temperature tensile strength and creep resistance of the Al alloy.

Compared with conventional cast eutectic Al alloys that contain a brittle micron-scale intermetallic network, LPBF refines eutectic spacing to a submicron scale and limits intermetallic size below 200 nm, achieving balanced room and high-temperature mechanical properties superior to commercial 2xxx and 7xxx wrought alloys [23]. With the further addition of Sc and Zr elements, coherent $L1_2$-Al_3(Sc, Zr) nanoparticles can precipitate within the Al matrix, creating a dual-scale synergistic strengthening consisting of a nano-eutectic skeleton with intragranular heat-resistant precipitates. This hybrid microstructure further enhances the deformability of the soft α-Al matrix and mitigates high-temperature softening [23].

Nevertheless, the nano-eutectic skeleton strategy based on rapid solidification still faces engineering limitations. An excessively high-volume fraction of the eutectic phase tends to induce hot cracking during LPBF processing, whereas an insufficient solute content fails to form a complete and continuous reinforcing network.

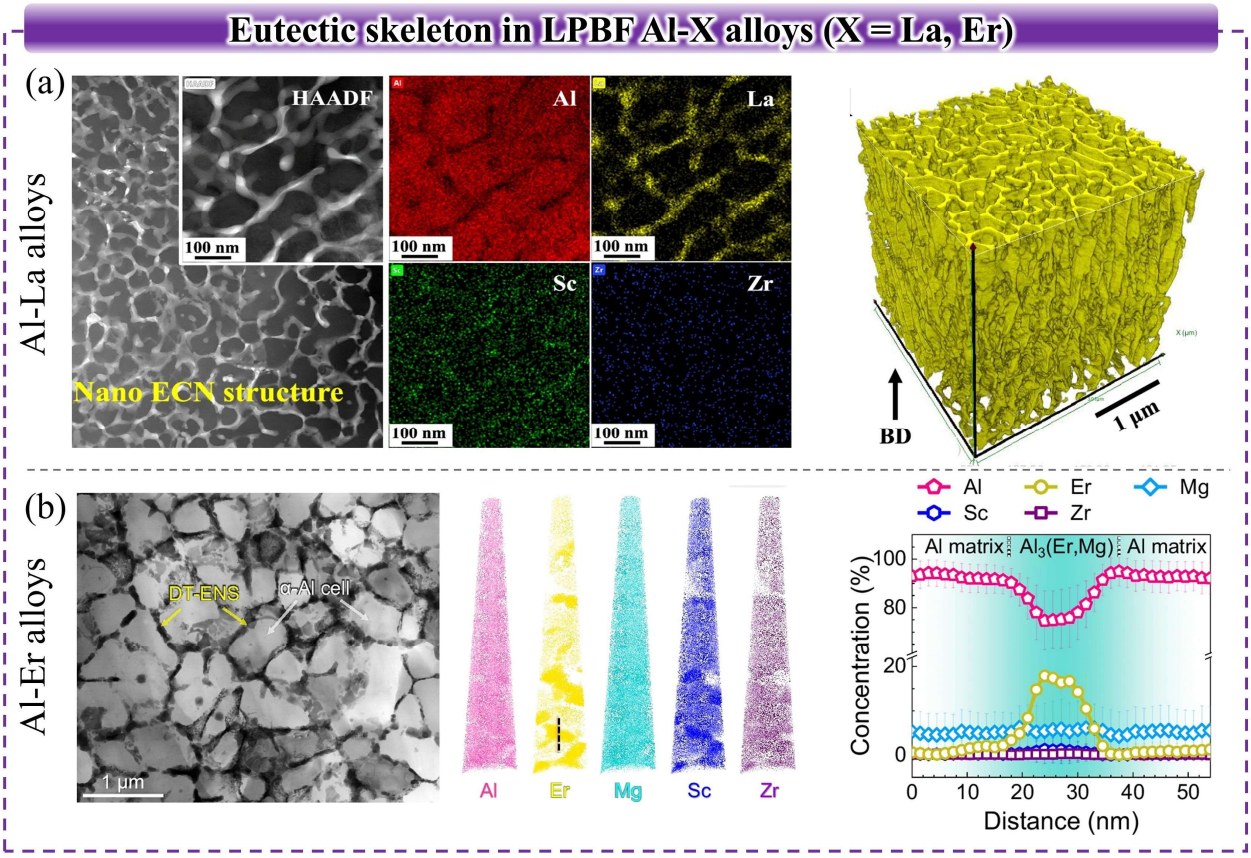

Figure 7. Microstructures of eutectic skeleton in LPBF-fabricated Al alloys: (**a**) Al–La–Sc–Zr alloys (Reprinted with permission from Ref. [23]. Copyright 2025, Springer Nature); (**b**) Al–Er–Mg alloys (the dashed line denotes the line-scan region). (Reprinted with permission from Ref. [18]. Copyright 2026, Springer Nature).

Table 2 directly compares core advantages, limitations, applicable temperature ranges, and potential trade-offs of microalloying, nanoparticle incorporation, and nano-eutectic skeleton strengthening mechanisms. Each strategy exhibits unique application boundaries and performance characteristics that determine its applicability to 200–400 °C intermediate-temperature service scenarios.

Overall, microalloying is the optimal choice for low-cost and large-scale components serving below 250 °C. Nanoparticle incorporation is competent for high-temperature service scenarios but is restricted by poor formability and high cost. Benefiting from the unique non-equilibrium solidification characteristics of LPBF, the nano-eutectic skeleton strategy achieves the best comprehensive performance in the target 250–

400 °C temperature window, providing a novel and feasible pathway for the development of next-generation lightweight high-temperature Al alloys.

Table 2. Performance comparison of three typical strengthening strategies for heat-resistant Al alloys.

Strengthening Strategy	Advantages	Limitations	Applicable Temperature Range	Potential Trade-Offs
Microalloying	Low cost/Mature process and good formability/Enhances low or medium-temperature strength for mass production	Thermal instability of precipitates above 250 °C degrades strength and creep resistance	≤250 °C	Satisfactory low-temperature performance/Poor high-temperature structural stability
Nanoparticle incorporation	Stable nanoparticles/Improving high-temperature performance	Complex, costly PM process/Poor formability and easy particle agglomeration impair ductility	250–400 °C	Superior high-temperature performance at the cost of reduced ductility and manufacturability
Nano-eutectic skeleton	LPBF non-equilibrium solidification/Balancing high-temperature performance and design freedom	High powder and equipment cost/Low efficiency and inherent pore defects	250–400 °C	Best medium-high temperature performance/Limited by high cost and low scalability

3. Processing Technologies and Mechanical Properties of Heat-Resistant Al Alloys

Driven by the development of industrial technologies, the emergence of diverse innovative processing technologies has broadened the boundaries of compositional design and achievable mechanical properties for heat-resistant Al alloys. The following sections focus on three mainstream fabrication technologies for Al alloys, namely permanent mold casting (PMC), powder metallurgy (PM), and laser powder bed fusion (LPBF) (Figure 8).

3.1. Processing Technologies

PMC, PM, and LPBF represent three typical fabrication routes for heat-resistant Al alloys, each exhibiting distinctly different solidification behaviors and microstructural regulations. As an old manufacturing technology, PMC depends on the slow near-equilibrium solidification. This technique features ultra-low production costs and great feasibility of fabricating large components with complex internal cavities. However, its intrinsically low cooling rate inevitably generates coarse dendrites, remarkable elemental segregation, and characteristic casting defects, including shrinkage porosity and hot tearing [47]. For conventional age-hardened cast Al alloys, nano-scaled precipitates readily undergo rapid coarsening and dissolution at temperatures exceeding 200 °C, which makes such alloys inadequate for long-term service of aerospace structural components working at 200–400 °C.

A key branch of PM is the nanoparticle-incorporation strengthening route, which introduces thermally stable ceramic nanoparticles into the metal through solid-state mechanical alloying and sintering [48]. These homogeneously dispersed nanoparticles exert a strong pinning effect on grain boundaries and dislocations, giving alloys markedly superior creep resistance compared to cast alloys. However, it is inherently limited in fabricating complex, lightweight components. Moreover, the traditional powder metallurgy route comprises several steps: mechanical alloying of composite powders, consolidation by sintering, post-consolidation heat treatment, and final machining. The complex multi-step manufacturing process incurs extremely high production costs, hindering widespread industrial adoption. With the development of additive manufacturing, powder-based AM represents a promising production route for

nanoparticle-incorporation strengthening materials, as it enables direct near-net-shape consolidation from customized powder feedstocks, thereby significantly shortening the manufacturing process.

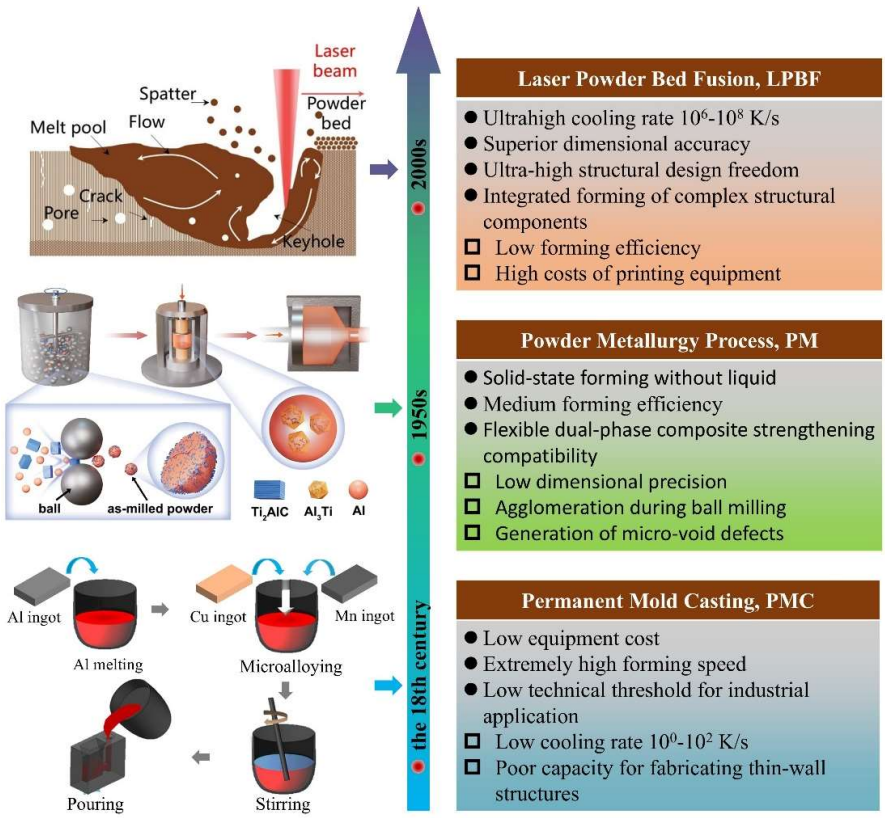

Figure 8. Schematics and processing characteristics of the fabrication route. Laser powder bed fusion (LPBF), powder metallurgy process (PM) (Reprinted with permission from Ref. [22]. Copyright 2026, Springer Nature), and permanent mold casting (PMC).

LPBF achieves ultrahigh cooling rates of 10^6–10^8 K/s during layer-by-layer laser melting, which effectively suppresses the formation of coarse equilibrium intermetallics and facilitates the development of nano-eutectic and crystalline-amorphous hybrid microstructures with exceptional thermal stability [16,20]. Taking advantage of digital manufacturing, LPBF offers superior dimensional accuracy and outstanding design freedom, enabling the fabrication of complex high-temperature components with conformal cooling channels and lattice architectures. Nevertheless, drawbacks include low printing efficiency, high spherical powder and equipment costs, as well as hard-to-eliminate pore and hot cracking defects that restrict industrialization.

PMC, PM, and LPBF exhibit differences in terms of processing cost, production efficiency, raw-material cost, scalability, and industrial maturity. PMC presents the lowest raw material and processing costs, superior production efficiency, and the highest level of industrial maturity, whereas it suffers from limited compositional flexibility, coarse microstructures, and inherent casting defects. Conventional PM involves multiple manufacturing procedures, resulting in relatively higher material and processing costs, while delivering moderate efficiency and scalability for components with simple geometries. LPBF possesses the highest overall manufacturing cost due to the expensive spherical powder feedstock, low deposition rate, and extensive post-processing requirements, which severely restrict its industrial scalability. Although the industrial maturity of LPBF is continuously improving, it still lags behind conventional PMC and PM technologies. In summary, PMC serves as the most cost-effective solution for mass production. PM provides a feasible compromise between mechanical performance and manufacturing cost. LPBF achieves unprecedented structural design freedom and remarkable microstructure refinement at the expense of high cost and low productivity. The selection of the optimal manufacturing strategy depends on the

practical application scenario and requires a comprehensive balance between service performance requirements and economic benefits.

3.2. Tensile Properties

Figure 9 systematically compares the balance between tensile strength and elongation of heat-resistant Al alloys fabricated by conventional PMC, PM, and LPBF at 25 °C, 250 °C, 300 °C, and 400 °C. At room temperature, benefiting from the unique process characteristics of LPBF and PM, Al alloys exhibit substantially higher tensile strength than their cast counterparts while retaining moderate ductility. In the intermediate temperature regime of 250–300 °C, LPBF demonstrates a superior strength-ductility synergy over the other two routes. As shown in Figure 9b,c, LPBF Al alloys achieve a more favorable combination of tensile strength and elongation in the 250–300 °C range compared with their PMC and PM counterparts. This improved strength-ductility synergy can be attributed to the unique microstructural features induced by LPBF, including ultrafine cellular structures, supersaturated solid solutions, and refined eutectic networks, which collectively enhance both work hardening capacity and resistance to localized deformation. LPBF Al alloys offer a wider range of achievable ductility while maintaining competitive tensile strength, whereas cast Al alloys suffer a pronounced degradation in high-temperature strength. Although PM Al alloys exhibit a marginal advantage in high-temperature strength stability, the ductility remains consistently low at elevated temperatures. Under the extreme condition of 400 °C, both LPBF and PM alloys display the best strength retention capability, while cast Al alloys exhibit the poorest load-bearing capacity. Overall, LPBF and PM routes are more suitable for components that demand high strength at room or intermediate temperatures, provided attention is paid to improving elongation. Conventional casting is appropriate for parts with modest strength requirements where cost control is the primary concern.

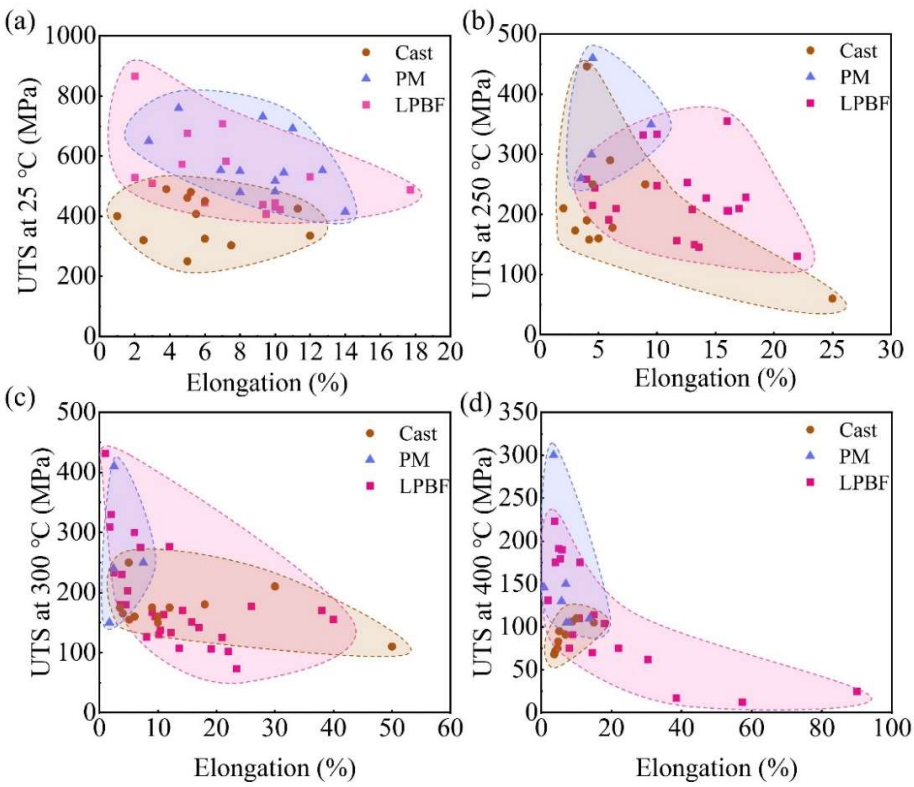

Figure 9. Performance summary of heat-resistant Al alloys at (**a**) room-temperature; (**b**) 250 °C; (**c**) 300 °C; (**d**) 400 °C. (Adapted with permission from Ref. [2,5,20,21,23,32,46,49–59]. Copyright 2023, 2026, 2025, 2024, and 2025, Elsevier, Springer Nature, Taylor & Francis).

3.3. Creep Properties

For a heat-resistant Al alloy component, long-term service under constant loading at 200–400 °C makes creep deformation and stress rupture the dominant failure modes. Accordingly, high-temperature creep performance is a critical metric for evaluating the practical service capability of Al alloys. Figure 10 provides a summary of the creep properties of various Al alloys.

For Al–Si alloys, Si precipitates undergo rapid spheroidization and coarsening above 225 °C [58], thereby significantly accelerating creep rates and degrading creep resistance under prolonged loading. For Al–Cu alloys, metastable θ′ strengthening precipitates tend to coarsen at elevated temperatures. Meanwhile, precipitate-free zones form during creep, accelerating creep damage accumulation [60]. The addition of transition metals such as Sc and Zr can substantially improve the thermal stability and high-temperature strengthening capacity of Al alloys [61]. For example, Al–Mg–Sc–Zr alloys exhibit outstanding intermediate-temperature creep resistance, attributed to the $L1_2$-ordered Al_3(Sc, Zr) nanoprecipitates that pin dislocations and suppress dislocation climb. However, prolonged high-temperature aging leads to coarsening of these nano-scale precipitates, thereby weakening creep resistance.

Existing creep investigations have largely focused on eutectic Al alloys, including Al–Ce and Al–Fe alloys. These eutectic alloys contain thermally stable intermetallic networks (e.g., $Al_{11}Ce_3$, Al_9(Ni, Fe), and quasi-crystalline phases) that effectively impede grain boundary sliding and dislocation climb at 300–400 °C, imparting superior long-term creep stability [62,63]. For instance, Li et al. [20] have fabricated an Al–Fe–V–Si–Ti alloy with a steady-state creep rate on the order of 10^{-8} s^{-1} at 300 °C under applied stresses of 100 MPa and 150 MPa, representing a reduction of one to three orders of magnitude compared with most other Al alloys. Additionally, although ceramic particle-reinforced Al matrix composites achieve enhanced room-temperature strength, interfaces between ceramic reinforcements and the Al matrix act as preferential void nucleation sites during creep, severely degrading high-temperature ductility [64].

Overall, systematic studies on the creep behavior of heat-resistant Al alloys remain insufficient. Most available creep data originate from short-duration tests, while long-term creep data spanning thousands of hours are rarely reported. Current alloy systems generally suffer from two key drawbacks: low creep ductility and excessively high steady-state creep rates under high applied stresses. Future research should prioritize the regulation of thermally stable precipitates to design novel heat-resistant Al alloys that simultaneously possess high tensile strength and outstanding long-term creep resistance.

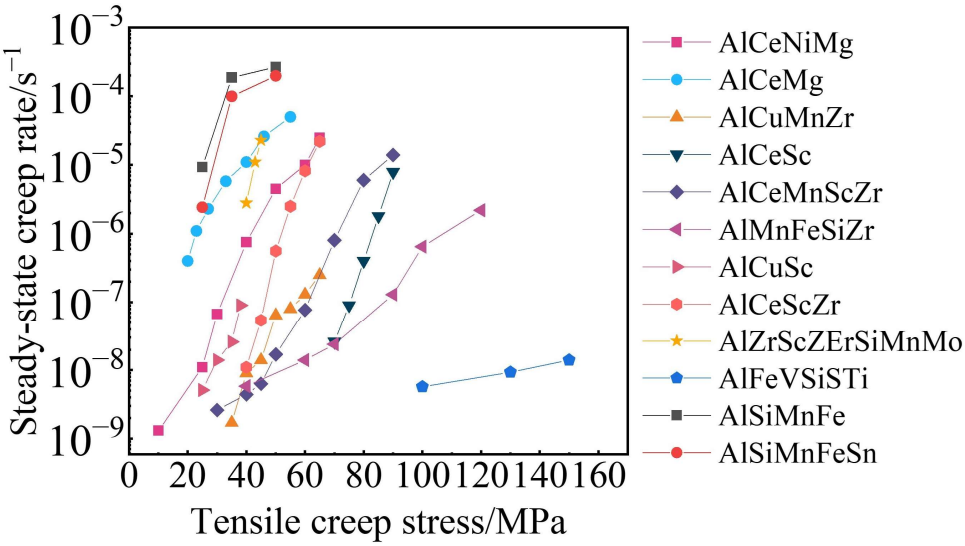

Figure 10. Steady-state creep rates of Al alloys under various stress levels at 300 °C (Adapted with permission from Ref. [14,20,41,65–67]. Copyright 2019, Taylor & Francis, Elsevier, and Springer Nature).

4. Conclusions and Prospects

This review systematically summarizes three mainstream microstructural regulation strategies for heat-resistant Al alloys, and compares the microstructural characteristics and mechanical performance of heat-resistant Al alloys fabricated by permanent mold casting (PMC), powder metallurgy (PM), and laser powder bed fusion (LPBF). The main conclusions are drawn as follows:

1. Microalloying remains the dominant strategy for improving the thermal stability of Al alloys through the formation of thermally stable precipitates, composite interfacial segregation, and solute-vacancy multidimensional confinement. Powder metallurgy-based nanoparticle incorporation provides an alternative, effective strengthening route via the uniform dispersion of high-melting ceramic nanoparticles. In particular, LPBF-induced continuous nano-eutectic skeletons create a unique complementary microstructure design, enabling superior medium-temperature and high-temperature performance that is inaccessible for traditional fabrication methods.
2. Three manufacturing techniques exhibit distinct performance and industrial trade-offs. Permanent mold casting (PMC) delivers outstanding cost effectiveness and high industrial maturity but produces alloys with coarse microstructures and inferior high-temperature mechanical stability. Powder metallurgy (PM) achieves excellent elevated-temperature strength via nanoparticle strengthening, whereas its application is restricted by complicated processing procedures, high manufacturing costs, and limited structural formability. By ultrahigh cooling rates and non-equilibrium solidification, LPBF enables the fabrication of heat-resistant Al alloys with well-balanced strength and ductility at 200–400 °C, though it suffers from high raw material cost, low production scalability, and inherent printing defects.
3. Future efforts should focus on further promoting the engineering applications of heat-resistant Al alloys capable of long-term service at 200–400 °C. Specifically, five promising research directions are highlighted: (i) development of low-cost alloying systems with reduced rare-earth or expensive elemental additions to improve industrial scalability; (ii) exploration of multiscale composite strengthening strategies by tailoring precipitates and eutectic network structures for upgraded thermal stability; (iii) establishment of systematic long-term service evaluation systems under thermal-mechanical coupling and cyclic loading conditions; (iv) control and elimination of LPBF defects through process optimization and post-treatment modification; (v) construction of standardized process-microstructure-property databases to support digital alloy design and industrial production.

Author Contributions

Y.-N.P.: Investigation, Data curation, Writing—Original Draft; H.-L.J.: Conceptualization, Methodology, Data Curation, Validation, Visualization, Supervision, Writing—Original Draft; T.-Y.L.: Investigation, Visualization; J.-W.S.: Investigation, Visualization; H.W.: Investigation, Visualization; M.Z.: Conceptualization, Methodology, Validation, Writing—Original Draft.

Ethics Statement

Not applicable.

Informed Consent Statement

Not applicable.

Data Availability Statement

No new data were generated in this study. All information supporting the findings of this review is available within the review.

Funding

This work was funded by the National Key Research and Development Program (No. 2024YFE0108900), National Natural Science Foundation of China (Nos. 52334010 and 52001133), Yunnan Fundamental Research Projects (No. 202601BC070008) and Key Research and Development Project of Linyi City (No. 2025PT008).

Declaration of Competing Interest

The authors declare that they have no known competing financial interests or personal relationships that could have appeared to influence the work reported in this paper.

References

1. Kang Z, Zhang Y. Materials science empowers carbon neutrality. *Natl. Sci. Open* **2024**, *3*, 20240057. DOI:10.1360/nso/20240057
2. Wang W, Takata N, Suzuki A, Kobashi M, Kato M. Design of Al–Fe–Mn alloy for both high-temperature strength and sufficient processability of laser powder bed fusion. *Addit. Manuf.* **2023**, *68*, 103524. DOI:10.1016/j.addma.2023.103524
3. Qu Z, Zhang Z, Liu R, Xu L, Zhang Y, Li X, et al. High fatigue resistance in a titanium alloy via near-void-free 3D printing. *Nature* **2024**, *626*, 999–1004. DOI:10.1038/s41586-024-07048-1
4. Yang X, Li R, Yuan T, Ke L, Bai J, Yang K. A comprehensive overview of additive manufacturing aluminum alloys: Classifications, structures, properties and defects elimination. *Mater. Sci. Eng. A* **2025**, *919*, 147464. DOI:10.1016/j.msea.2024.147464
5. Piao YN, Jia HL, Zha M, Ma PK, Gao D, Yin CR, et al. The effect of quenching rates on microstructure and mechanical properties of an Al–Si–Cu–Mg alloy. *Mater. Charact.* **2023**, *196*, 112609. DOI:10.1016/j.matchar.2022.112609
6. Zhu Z, Ng FL, Seet HL, Lu W, Liebscher CH, Rao Z, et al. Superior mechanical properties of a selective-laser-melted AlZnMgCuScZr alloy enabled by a tunable hierarchical microstructure and dual-nanoprecipitation. *Mater. Today* **2022**, *52*, 90–101. DOI:10.1016/j.mattod.2021.11.019
7. Wu S, Soreide HS, Chen B, Bian J, Yang C, Li C, et al. Freezing solute atoms in nanograined aluminum alloys via high-density vacancies. *Nat. Commun.* **2022**, *13*, 3495. DOI:10.1038/s41467-022-31222-6
8. Wang Y, Xia X, Li R, Wang T, Yuan T. A review of additive manufacturing heat-resistant aluminum alloys: Materials, properties and strengthening strategies at high temperature. *Int. Mater. Rev.* **2025**, *70*, 648–709. DOI:10.1177/09506608251369181
9. Li K, Zhan J, Wang Y, Qin Y, Gong N, Zhang DZ, et al. Application of data-driven methods for laser powder bed fusion of Ni-based superalloys: A review. *J. Manuf. Process.* **2025**, *133*, 285–321. DOI:10.1016/j.jmapro.2024.11.053
10. Williams JC, Starke EA. Progress in structural materials for aerospace systems. *Acta Mater.* **2003**, *51*, 5775–5799. DOI:10.1016/j.actamat.2003.08.023
11. Bahl S, Wu T, Michi RA, An K, Yu D, Allard LF, et al. An additively manufactured near-eutectic Al–Ce–Ni–Mn–Zr alloy with high creep resistance. *Acta Mater.* **2024**, *268*, 119787. DOI:10.1016/j.actamat.2024.119787
12. Kerni L, Raina A, Haq MIU. Performance evaluation of aluminium alloys for piston and cylinder applications. *Mater. Today Proc.* **2018**, *5*, 18170–18175. DOI:10.1016/j.matpr.2018.06.153
13. GhasemiPourMasoule SH, Keshavarzi A, Saeidi Googarchin H. A review on structural and mechanical insights into electric vehicle battery packs: Subsystems, standards, and design innovations. *J. Energy Storage* **2026**, *158*, 121657. DOI:10.1016/j.est.2026.121657
14. Gao YH, Yang C, Zhang JY, Cao LF, Liu G, Sun J, et al. Stabilizing nanoprecipitates in Al–Cu alloys for creep resistance at 300 °C. *Mater. Res. Lett.* **2019**, *7*, 18–25. DOI:10.1080/21663831.2018.1546773
15. Rosalie JM, Bourgeois L. Silver segregation to θ′ (Al_2Cu)–Al interfaces in Al–Cu–Ag alloys. *Acta Mater.* **2012**, *60*, 6033–6041. DOI:10.1016/j.actamat.2012.07.039
16. Tang X, Zhang H, Xue P, Wu L, Zhang J, Zhang L, et al. Ultrahigh strength heat-resistant Al–Fe–V–Si–Sc alloy fabricated by laser powder bed fusion. *J. Mater. Sci. Technol.* **2025**, *239*, 299–306. DOI:10.1016/j.jmst.2025.02.060
17. Liu H, Gu D, Xi L, Zhang H, Shi K, Wu B, et al. High-Performance Aluminum-Based Materials Processed by Laser Powder Bed Fusion: Process, Microstructure, Defects and Properties Coordination. *Addit. Manuf. Front.* **2024**, *3*, 200145. DOI:10.1016/j.amf.2024.200145

18. Li Y, Chen T, Zhong S, Fang H, Sheng P, Ma S, et al. Strong 3D-printed aluminium reinforced with ductile-transformable eutectic nano-skeleton. *Nat. Commun.* **2026**, *17*, 5708. DOI:10.1038/s41467-026-72256-4
19. Li G, Huang Y, Zhao C, He X, Wang S, Tan Q, et al. Strong yet ductile heat-resistant aluminum alloy by additive manufacturing. *Nat. Commun.* **2026**, *17*, 5230. DOI:10.1038/s41467-026-71926-7
20. Li M, Liu M, Li G, Liu Z, Fang F, Ma C, et al. 3-D printed ultrastrong heat-resistant aluminum alloy achieved by bioinspired nanoscale amorphous confinement. *Mater. Today* **2026**, *95*, 103267. DOI:10.1016/j.mattod.2026.103267
21. Wang Y, Yu C, Gan K, Yuan T, Li R. Intrinsic attraction driving the high temperature performance of additively manufactured aluminum alloys. *Nat. Commun.* **2026**, *17*, 4931. DOI:10.1038/s41467-026-71390-3
22. Hu HJ, Shi YH, Zan YN, Song M, Wang D, Wang QZ, et al. Hierarchical reinforcement strategy enables aluminum matrix composites with uncompromised high-temperature mechanical properties. *Nat. Commun.* **2026**, *17*, 6407. DOI:10.1038/s41467-026-73160-7
23. Ma S, Chen Z, Fang H, Ji G, Wang M, Cui Y, et al. High-temperature strength in an additively manufactured Al-based superalloy with stable nanoscale eutectic cellular networks. *Nat. Commun.* **2025**, *16*, 11361. DOI:10.1038/s41467-025-66441-0
24. Chowdhury S, Yadaiah N, Prakash C, Ramakrishna S, Dixit S, Gupta LR, et al. Laser powder bed fusion: A state-of-the-art review of the technology, materials, properties & defects, and numerical modelling. *J. Mater. Res. Technol.* **2022**, *20*, 2109–2172. DOI:10.1016/j.jmrt.2022.07.121
25. Qiang W, Zhang X, Xu Z, Zhao D, Rong X, Shi C, et al. Dual heterogeneity design in high-strength Cu–Ti alloys via powder metallurgy for enhanced ductility and conductivity. *Mater. Res. Lett.* **2026**, *14*, 720–728. DOI:10.1080/21663831.2026.2651932
26. Khan MWA, Ahmad R, Bukhari SMA, Sultan M, Husnain N, Anwar MT, et al. Influence of Vibration-Assisted Dynamic Solidification on Microstructure and Mechanical Properties of Permanent Mold Cast Aluminum Alloy 2024 with Conformal Cooling. *J. Manuf. Mater. Process.* **2025**, *9*, 416. DOI:10.3390/jmmp9120416
27. Ekaputra CN, Rakhmonov JU, Senvardarli E, Weiss D, Mogonye JE, Dunand DC. Combining solution-, precipitation- and load-transfer strengthening in a cast Al–Ce–Mn–Sc–Zr alloy. *Acta Mater.* **2024**, *266*, 119683. DOI:10.1016/j.actamat.2024.119683
28. Xu JY, Zhang C, Liu LX, Guo R, Sun MJ, Liu L. Achieving high strength in laser powder-bed fusion processed AlFeCuZr alloy via dual-nanoprecipitations and grain boundary segregation. *J. Mater. Sci. Technol.* **2023**, *137*, 56–66. DOI:10.1016/j.jmst.2022.07.033
29. Martin JH, Yahata BD, Hundley JM, Mayer JA, Schaedler TA, Pollock TM. 3D printing of high-strength aluminium alloys. *Nature* **2017**, *549*, 365–369. DOI:10.1038/nature23894
30. Seidman DN, Marquis EA, Dunand DC. Precipitation strengthening at ambient and elevated temperatures of heat-treatable Al(Sc) alloys. *Acta Mater.* **2002**, *50*, 4021–4035. DOI:10.1016/S1359-6454(02)00201-X
31. Xiao YK, Yang Q, Bian ZY, Chen H, Wu Y, Lian Q, et al. Microstructure, heat treatment and mechanical properties of TiB_2/Al–7Si–Cu–Mg alloy fabricated by selective laser melting. *Mater. Sci. Eng. A* **2021**, *809*, 140951. DOI:10.1016/j.msea.2021.140951
32. Xue H, Yang C, De Geuser F, Zhang P, Zhang J, Chen B, et al. Highly stable coherent nanoprecipitates via diffusion-dominated solute uptake and interstitial ordering. *Nat. Mater.* **2023**, *22*, 434–441. DOI:10.1038/s41563-022-01420-0
33. Lu Q, Wang J, Li H, Jin S, Sha G, Lu J, et al. Synergy of multiple precipitate/matrix interface structures for a heat resistant high-strength Al alloy. *Nat. Commun.* **2023**, *14*, 2959. DOI:10.1038/s41467-023-38730-z
34. Bourgeois L, Dwyer C, Weyland M, Nie JF, Muddle BC. The magic thicknesses of θ′ precipitates in Sn-microalloyed Al–Cu. *Acta Mater.* **2012**, *60*, 633–644. DOI:10.1016/j.actamat.2011.10.015
35. Feng Q, Zhang P, Liu F, Xue H, Yang C, Xiang K, et al. Simultaneously improving strength and thermal stability of Al–Cu–Sc alloys through Cd micro-alloying. *Acta Mater.* **2026**, *309*, 122054. DOI:10.1016/j.actamat.2026.122054
36. Gao YH, Guan PF, Su R, Chen HW, Yang C, He C, et al. Segregation-sandwiched stable interface suffocates nanoprecipitate coarsening to elevate creep resistance. *Mater. Res. Lett.* **2020**, *8*, 446–453. DOI:10.1080/21663831.2020.1799447
37. Huang G, Pan S, Dong C, Chen Q, Fnu K, Li Z. Accelerated Hardening and Corrosion Behavior of Low Cu/Mg Al–Cu–Mg Alloys Modified by Si and Ag. *Metals* **2026**, *16*, 460. DOI:10.3390/met16050460
38. Mo YT, Xu XY, Liu ZT, Zhang HX, Wang C, Liu X, et al. Superior thermal stability in a high-strength Al–Zn–Mg–Cu–Si alloy via tailored precipitation sequence. *Mater. Res. Lett.* **2025**, *13*, 503–512. DOI:10.1080/21663831.2025.2475243
39. Gao YH, Liu G, Sun J. Recent progress in high-temperature resistant aluminum-based alloys: Microstructural design and precipitation strategy. *Acta Metall. Sin.* **2021**, *57*, 129–149. DOI:10.11900/0412.1961.2020.00347

40. Zhang X, Cheng F, Sun Y, Teng F, Shen H, Wang J. Mechanism controlling the thickening of T1 phase in an Al–Cu–Li–Mg–Ag alloy. *Mater. Res. Lett.* **2025**, *13*, 1208–1215. DOI:10.1080/21663831.2025.2569728
41. Michi RA, Sisco K, Bahl S, Yang Y, Poplawsky JD, Allard LF, et al. A creep-resistant additively manufactured Al–Ce–Ni–Mn alloy. *Acta Mater.* **2022**, *227*, 117699. DOI:10.1016/j.actamat.2022.117699
42. Jia Q, Zhuo Y, Yan Y, Lu C, Chen Z, Cheng Y, et al. Tensile creep mechanisms of Al–Mn–Sc alloy fabricated by additive manufacturing. *Addit. Manuf.* **2024**, *79*, 103910. DOI:10.1016/j.addma.2023.103910
43. Shin D, Wolverton C. First-principles study of solute–vacancy binding in magnesium. *Acta Mater.* **2010**, *58*, 531–540. DOI:10.1016/j.actamat.2009.09.031
44. Hirata A, Fujita T, Wen YR, Schneibel JH, Liu CT, Chen MW. Atomic structure of nanoclusters in oxide-dispersion-strengthened steels. *Nat. Mater.* **2011**, *10*, 922–926. DOI:10.1038/nmat3150
45. Smith TM, Kantzos CA, Zarkevich NA, Harder BJ, Heczko M, Gradl PR, et al. A 3D printable alloy designed for extreme environments. *Nature* **2023**, *617*, 513–518. DOI:10.1038/s41586-023-05893-0
46. Bai X, Xie H, Zhang X, Zhao D, Rong X, Jin S, et al. Heat-resistant super-dispersed oxide strengthened aluminium alloys. *Nat. Mater.* **2024**, *23*, 747–754. DOI:10.1038/s41563-024-01884-2
47. Pohl M, Teichmann F, Müller S. Investigations on the use of salt as a sustainable moulding material for AlSi12 gravity casting. *Mater. Today Commun.* **2026**, *52*, 115126. DOI:10.1016/j.mtcomm.2026.115126
48. Hou W, Stubbs T, DeBeer-Schmitt L, Chang YT, Charpagne MA, Smith TM, et al. Dissolution zone model of the oxide structure in additively manufactured dispersion-strengthened alloys. *Addit. Manuf.* **2024**, *96*, 104554. DOI:10.1016/j.addma.2024.104554
49. Zhu R, Chen W, Chen Z, Sui Y, Qu Y. Effect of combined addition of Ni and Sc on microstructure and high-temperature mechanical properties of an Al–Cu–Mn alloy. *J. Alloys Compd.* **2025**, *1023*, 179971. DOI:10.1016/j.jallcom.2025.179971
50. Su X, Lei Y, Chen Y, Qu H, Qi Z, Zheng G, et al. Precipitating thermally reinforcement phase in aluminum alloys for enhanced strength at 400 °C. *J. Mater. Sci. Technol.* **2024**, *172*, 71–82. DOI:10.1016/j.jmst.2023.06.038
51. Huang X, Huang T, Mishin OV, Zhu Y, Wu G, Huang X. Achieving superior high-temperature strength in nanostructured Al–Cu–Mn alloy with Sc addition. *Mater. Res. Lett.* **2026**, *14*, 186–194. DOI:10.1080/21663831.2025.2611736
52. Guan L, Liu K, Su Y, Dong Y, Li M, Cao H, et al. Defect-induced and deformation-mediated: A relay race-hardening strategy for high-content nanoparticle-reinforced aluminum matrix composites. *Compos. Part B Eng.* **2026**, *324*, 113848. DOI:10.1016/j.compositesb.2026.113848
53. Li D, Zhang Q, Gao K, Liu J, Chen Z, Wang H. Enhanced strength-ductility synergy and isotropy in TiB_2/Al composites through powder engineering. *Mater. Sci. Eng. A* **2025**, *946*, 149102. DOI:10.1016/j.msea.2025.149102
54. Chen J, Chen L, Li X, Ao Z, Zhao Y, Guo W, et al. Microstructural heterogeneity enabled balance of room- and high-temperature properties in high-volume intermetallics reinforced aluminum alloys. *Mater. Res. Lett.* **2026**, *14*, 12–19. DOI:10.1080/21663831.2025.2581228
55. Shang A, Stegman B, Choy K, Niu T, Shen C, Shang Z, et al. Additive manufacturing of an ultrastrong, deformable Al alloy with nanoscale intermetallics. *Nat. Commun.* **2024**, *15*, 5122. DOI:10.1038/s41467-024-48693-4
56. Wang G, Zhang Y, Liu J, Chen W, Wang K, Cui B, et al. Dispersion hardening using amorphous nanoparticles deployed via additive manufacturing. *Nat. Commun.* **2025**, *16*, 3589. DOI:10.1038/s41467-025-58893-1
57. Bahl S, Sisco K, Yang Y, Theska F, Primig S, Allard LF, et al. Al–Cu–Ce(–Zr) alloys with an exceptional combination of additive processability and mechanical properties. *Addit. Manuf.* **2021**, *48*, 102404. DOI:10.1016/j.addma.2021.102404
58. Uzan NE, Shneck R, Yeheskel O, Frage N. High-temperature mechanical properties of AlSi10Mg specimens fabricated by additive manufacturing using selective laser melting technologies (AM-SLM). *Addit. Manuf.* **2018**, *24*, 257–263. DOI:10.1016/j.addma.2018.09.033
59. Yu C, Xia X, Gan K, Wang T, Dong P, Liang X, et al. Potent interplay between $L1_2$ nanoprecipitates and 9R phase enabling strength-ductility synergy in a 650 MPa-class additively manufactured aluminum alloy. *Int. J. Plast.* **2026**, *197*, 104595. DOI:10.1016/j.ijplas.2025.104595
60. Michi RA, Bahl S, Fancher CM, Sisco K, Allard LF, An K, et al. Load shuffling during creep deformation of an additively manufactured AlCuMnZr alloy. *Acta Mater.* **2023**, *244*, 118557. DOI:10.1016/j.actamat.2022.118557
61. Bi J, Liu L, Wang C, Chen G, Jia X, Chen X, et al. Microstructure, tensile properties and heat-resistant properties of selective laser melted AlMgScZr alloy under long-term aging treatment. *Mater. Sci. Eng. A* **2022**, *833*, 142527. DOI:10.1016/j.msea.2021.142527
62. Rakhmonov JU, Weiss D, Dunand DC. Solidification microstructure, aging evolution and creep resistance of laser powder-bed fused Al–7Ce–8Mg (wt%). *Addit. Manuf.* **2022**, *55*, 102862. DOI:10.1016/j.addma.2022.102862

63. Wu T, Poplawsky JD, Allard LF, Plotkowski A, Shyam A, Dunand DC. Microstructure and strengthening of Al–6Ce–3Ni–0.7Fe (wt%) alloy manufactured by laser powder-bed fusion. *Addit. Manuf.* **2023**, *78*, 103858. DOI:10.1016/j.addma.2023.103858
64. Feng S, Li Q, Liu W, Shu G, Wang X. Microstructure and mechanical properties of Al–B_4C composite at elevated temperature strengthened with in situ Al_2O_3 network. *Rare Met.* **2020**, *39*, 671–679. DOI:10.1007/s12598-019-01279-2
65. Kloc L, Spigarelli S, Cerri E, Evangelista E, Langdon TG. Creep behavior of an aluminum 2024 alloy produced by powder metallurgy. *Acta Mater.* **1997**, *45*, 529–540. DOI:10.1016/S1359-6454(96)00190-5
66. Rakhmonov JU, Vo NQ, Croteau JR, Dorn J, Dunand DC. Laser-melted Al–3.6Mn–2.0Fe–1.8Si–0.9Zr (wt%) alloy with outstanding creep resistance via formation of α-Al(FeMn)Si precipitates. *Addit. Manuf.* **2022**, *60*, 103285. DOI:10.1016/j.addma.2022.103285
67. Wang R, Chen H, Wang D, Nagaumi H, Shi H, Zhang M, et al. Improving high-temperature creep resistance in Al–Si cast alloy by trace Sn-induced high number density dispersoids. *Mater. Charact.* **2025**, *229*, 115634. DOI:10.1016/j.matchar.2025.115634